



**HAL**  
open science

## Non-covalent interactions in neutral and oxidized tetrathiafulvalenes

Haia Kharraz, Hadi Hachem, Yann Le Gal, Thierry Roisnel, Olivier Jeannin, Frédéric Barrière, Thierry Guizouarn, Dominique Lorcy

► **To cite this version:**

Haia Kharraz, Hadi Hachem, Yann Le Gal, Thierry Roisnel, Olivier Jeannin, et al.. Non-covalent interactions in neutral and oxidized tetrathiafulvalenes. *CrystEngComm*, 2023, 25 (19), pp.2946-2958. 10.1039/d3ce00257h . hal-04115676

**HAL Id: hal-04115676**

**<https://hal.science/hal-04115676v1>**

Submitted on 2 Jun 2023

**HAL** is a multi-disciplinary open access archive for the deposit and dissemination of scientific research documents, whether they are published or not. The documents may come from teaching and research institutions in France or abroad, or from public or private research centers.

L'archive ouverte pluridisciplinaire **HAL**, est destinée au dépôt et à la diffusion de documents scientifiques de niveau recherche, publiés ou non, émanant des établissements d'enseignement et de recherche français ou étrangers, des laboratoires publics ou privés.







Distributed under a Creative Commons Attribution - NonCommercial 4.0 International License



Cite this: *CrystEngComm*, 2023, 25, 2946

## Non-covalent interactions in neutral and oxidized tetrathiafulvalenes†

Haia Kharraz, Hadi Hachem, Yann Le Gal, Thierry Roisnel,  Olivier Jeannin,  Frédéric Barrière,  Thierry Guizouarn and Dominique Lorcy \*

Tetrathiafulvalenes (TTFs) functionalized with groups able to increase non-covalent intermolecular interactions through either hydrogen, halogen or chalcogen bonding were investigated. For that purpose, we designed several appropriate precursors, fused dithiole-2-one/thiazoles, which under homocoupling led to symmetrically substituted TTFs or through heterocoupling to dissymmetrically substituted TTFs. The electrochemical investigations allowed the assessment of the electronic effect of these substituents on the overall donating ability of the TTFs. In addition two charge transfer salts have been prepared involving two of these TTFs with TCNQF<sub>4</sub> as the electron acceptor, (4c)<sub>2</sub>(TCNQF<sub>4</sub>) and (4b)(TCNQF<sub>4</sub>). Furthermore the crystal structures of the neutral TTFs and of the charge transfer salts allowed us to study the stacking mode and the different non-covalent interactions taking place in the crystals, in connection with the calculated electrostatic surface potential (ESP) of the investigated molecules. All the data provide information about non-covalent bonding interactions in the solid state and about their potential contribution to direct to some extent crystallographic intermolecular organization.

Received 15th March 2023,  
Accepted 24th April 2023

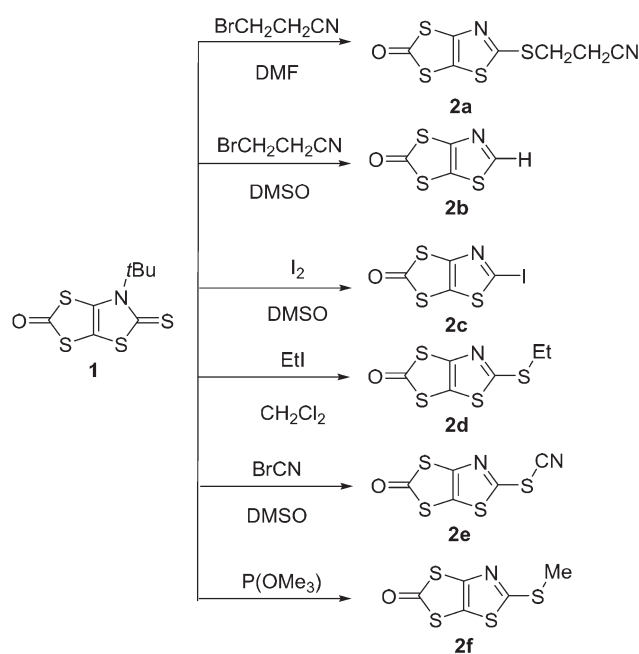
DOI: 10.1039/d3ce00257h

rsc.li/crystengcomm

## Introduction

For five decades now, tetrathiafulvalenes (TTF), a fascinating family of electron donor molecules, have been the focus of a great deal of interest as precursors of conducting molecular materials especially after the discovery of the first organic metal (TTF)(TCNQ).<sup>1,2</sup> In addition, remarkable redox properties make them valuable building blocks for a broad range of applications.<sup>3–6</sup> The properties of molecular materials are essentially linked to the organization and the interactions of the molecules in the solid state and it is somehow a big challenge to increase the dimensionality of these materials.<sup>7</sup> Indeed it is always difficult to predict how the molecules will be organized and interact within the material. Thereby, with the aim of gaining control over the intermolecular architecture, the use of non-covalent intermolecular interactions can be envisioned. For instance, hydrogen bonding interactions (HB),<sup>8</sup> first used by Bryce in 1995,<sup>9</sup> led to a catechol-fused ethylenedithio-TTF semiconducting material at ambient pressure, while upon application of pressure a metallic behavior was observed.<sup>10</sup> Among the various possible non-covalent interactions, halogen bonding (XB)<sup>11</sup> has also been investigated in order to

favor the organization of the TTFs in the solid state.<sup>12,13</sup> More recently, chalcogen bonding (ChB)<sup>14</sup> have focused also attention in this research area.<sup>15</sup> An interesting characteristic of these non-covalent interactions is that when the hydrogen,



**Scheme 1** Reactivity of N-tBu-1,3-thiazoline-2-thione derivative **1** towards various reagents.

Univ Rennes, CNRS, ISCR (Institut des Sciences Chimiques de Rennes) – UMR 6226, F-35000 Rennes, France. E-mail: dominique.lorcy@univ-rennes1.fr

† Electronic supplementary information (ESI) available. CCDC 2245494–2245502. For ESI and crystallographic data in CIF or other electronic format see DOI: <https://doi.org/10.1039/d3ce00257h>



halogen or chalcogen atoms are located on an electroactive moiety such as TTF, the lower electronic density called  $\sigma$ -hole, located on the extension of the covalent bond,<sup>16</sup> is enhanced upon oxidation. Indeed neutral TTF, substituted by a halogen or chalcogen atom, is an electron donor molecule, but once oxidized, the TTF exerts an electron withdrawing effect that increases the magnitude of the  $\sigma$ -hole and thus favor such intermolecular interactions. Herein we investigate the synthesis of novel substituted TTFs able to form non-covalent intermolecular interactions, such as hydrogen, halogen, or chalcogen bonding. We studied the influence of these non-covalent interactions in the solid state either on the precursors or on the neutral and oxidized TTFs.

## Results and discussion

In order to prepare the appropriate precursors of the targeted TTFs, we used *N*-*t*Bu-1,3-thiazoline-2-thione **1** as starting materials (Scheme 1).<sup>17</sup> Indeed, we have shown previously that compound **1** in the presence of an electrophile such as an halogenated alkyl can be converted into the 2-alkylthio-1,3-thiazole derivative.<sup>17,18</sup> Moreover, it is also possible to generate the 2-iodo-substituted thiazole core, by reacting **1** with iodine in DMSO forming the non-substituted thiazole core as a side product.<sup>19</sup> Thus we decided to explore the reactivity of **1** towards other reagents with the aim of preparing functionalized moieties which could bring the TTF core with a sizeable potential for non-covalent intermolecular interactions. We first focused on the cyanoethylthio functionalization. Indeed, the cyanoethyl group is an excellent protecting group of the thiolate.<sup>20</sup> Therefore, this protecting group can be withdrawn at will and replaced by other functional groups. For that purpose, the transformation of the *N*-*t*Bu-1,3-thiazoline-2-thione **1** into 2-cyanoethylthio-1,3-thiazole derivative **2a** was first studied in DMF. The reaction of **1** in DMF in the presence of an excess of bromopropionitrile led after 48 hours under inert atmosphere at 70 °C to the desired 2-cyanoethylthio-1,3-thiazole derivatives **2a** in 63% yield. We also attempted the same reaction using DMSO instead of DMF. Unexpectedly, using DMSO in the presence of **1** and an excess of bromopropionitrile, we isolated the non-substituted thiazole ring **2b** in 55% yield. We also prepared the iodo substituted precursor **2c** according to the procedure described earlier by simply mixing **1** with an excess of iodine in DMSO at 55 °C for four hours under inert atmosphere.<sup>19</sup>

The 2-ethylthio derivative **2d** was prepared by simply refluxing **1** for 2 hours with an excess of iodoethane in dichloromethane as previously reported.<sup>17</sup> The same procedure with cyanogen bromide (BrCN) as alkylating agent was not successful in dichloromethane while when the reaction was performed in DMSO at 55 °C for 16 h, the thiocyanate substituted precursor **2e** was isolated in 50% yield.

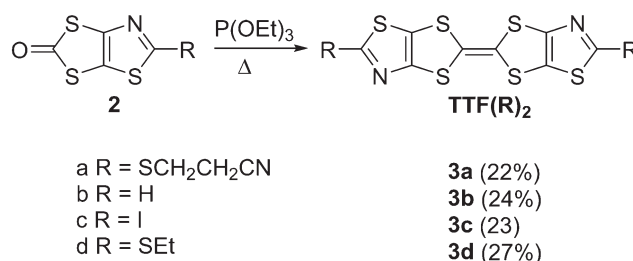
Dithiole-2-ones are known to be excellent precursors for the synthesis of TTF through their homocoupling, at 120 °C

under inert atmosphere, either in the presence of a phosphite derivative only, such as triethylphosphite or trimethylphosphite, or by mixing the dithiole-2-one in toluene in the presence of the trialkylphosphite.<sup>21</sup> Thus we investigated the reactivity of the different dithiole-2-one **1** and **2a–e** in the presence of trialkylphosphite. The first attempt concerns the coupling of the dithiole-2-one **1** in the presence of trimethylphosphite P(OMe)<sub>3</sub>, acting as solvent and reagent (Scheme 1). After several hours we did not observe the formation of the desired TTF but instead we isolated the 2-methylthio-1,3-thiazole derivative **2f** (Scheme 1). Therefore, in the presence of P(OMe)<sub>3</sub>, alkylation of the exocyclic sulfur occurs followed by the loss of the *t*Bu substituent. It is worth noting that the same compound **2f** was previously obtained by simply refluxing **1** with an excess of iodomethane in dichloromethane.<sup>17</sup>

Then we studied the reactivity of the dithiole-2-one **2a–d** with different substituents on position 2 of the thiazole ring toward homocoupling. These building blocks heated at 120 °C for 5 h in triethylphosphite P(OEt)<sub>3</sub> afforded the desired symmetric TTFs, **3(a–d)**, in relatively low yield after purification by column chromatography on silica gel (22–27% yield), Scheme 2.

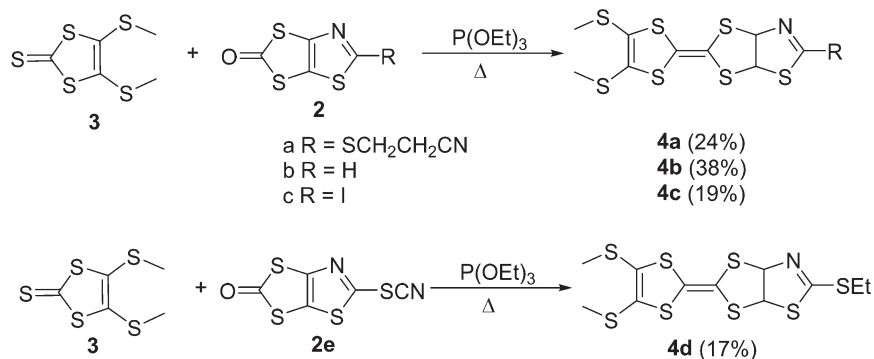
We also investigated the formation of dissymmetrically substituted TTF and for that purpose we chose the 4,5-bis(methylthio)-1,3-dithiole-2-thione **3** as the second building block in order to gain some solubility compared to the symmetrically substituted TTFs. Moreover, this dithiole-2-thione motif is known to have a low reactivity towards itself in the conditions used to form a TTF core and thus, the cross-coupling reaction toward unsymmetrical TTFs should be favored.<sup>22</sup> We carried out the cross-coupling reaction between the dithiole-2-one **3** and each of the four thiazole derivatives **2a–c** and **2e** in the same conditions, *i.e.* 2 hours at 120 °C in P(OEt)<sub>3</sub> (Scheme 3). Besides for **2e**, all the expected dissymmetrical TTF, **4a–c**, are formed (19–38% yield). Using this approach no symmetrical TTF, **3a–c**, was isolated. In the case of **2e** the only TTF which could be isolated is the dissymmetrical TTF, **4d**.

Here again we attempted the cross-coupling reaction between the fused dithiole-2-one thiazoline **1** with **3** in P(OEt)<sub>3</sub> for 2 hours at 120 °C (Scheme 4). In these conditions, we isolated TTF **4d** in 46% yield. According to what we observed previously, a plausible explanation would be that thiazoline **1** in the presence of P(OEt)<sub>3</sub> is first transformed

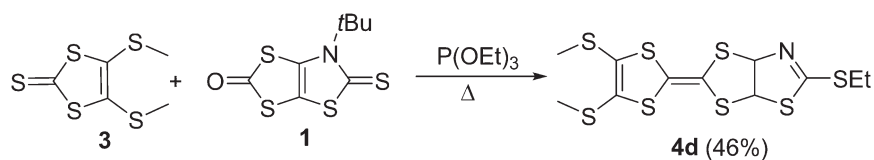


Scheme 2 Synthesis of symmetrical TTF(R)<sub>2</sub>.





**Scheme 3** Synthesis pathways of dissymmetrical TTF **4a-d**.



**Scheme 4** Reactivity of **1** in the presence of dithiole-2-thione **3** and P(OEt)<sub>3</sub>.

into the thiazole **2d** and then the heterocoupling occurs between **2d** and **3** to afford TTF **4d**.

Thus, in order to achieve the synthesis of the thiocyanate TTF **4e**, we used another approach that relies on the use of the protected TTF thiolate namely **4a**. The cyanoethyl group can indeed be easily removed in basic medium by adding caesium hydroxide to a DMF solution of TTF **4a** and after stirring for 30 min at room temperature cyanogen bromide (BrCN) was added. TTF **4e** was obtained in 70% yield after purification by chromatography on silica gel (Scheme 5). Thus we successfully synthesized various TTFs substituted either with hydrogen atoms, **3b** and **4b**, or with iodine atoms, **3c** and **4c**, susceptible to participate respectively into hydrogen or halogen bonding interactions. On the other hand, the nitrile on the sulfur atom of **4e** should increase the charge depletion on one  $\sigma$ -hole of this atom, in the prolongation of the NC-S bond, and potentially promote the formation of chalcogen bonding.

### Electrochemical investigation

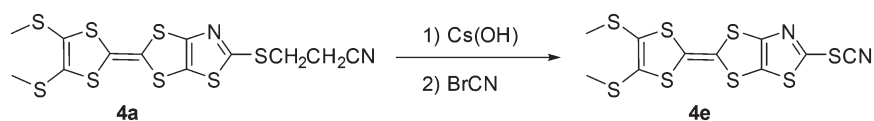
The redox properties of the TTF derivatives were investigated by cyclic voltammetry (CV) and the redox potentials are listed in Table 1 together with those of the tetramethylthio-TTF (MeS)<sub>4</sub>-TTF for comparison. All these TTFs exhibit a typical cyclic voltammogram for a TTF, namely two reversible oxidation waves corresponding to the successive oxidation of

the neutral TTF into the radical cation and then to the dication. The redox potentials of all the investigated TTFs are shifted to higher oxidation potentials than those observed for (MeS)<sub>4</sub>-TTF (Table 1). This anodic shift is more pronounced for the symmetrically substituted TTFs than for the dissymmetrically one indicating the electron withdrawing effect of the fused thiazole ring on the electron donating ability of the TTFs. Depending on the substituent on the thiazole ring, the same order from the easier to oxidize to the most difficult one is observed, either in the symmetrical series or in the dissymmetrical one, namely: SEt, SCH<sub>2</sub>CH<sub>2</sub>CN, H, I (**d**, **a**, **b**, **c**).

### Solid state investigations

Crystals suitable for X-ray diffraction studies were obtained by slow evaporation of concentrated dichloromethane solution of the three dithiole-2-one **2a**, **2e** and **2f**. The molecular structure of **2a**, **2e** and **2f** are presented in Fig. 1. In all cases the fused heterocycles (dithiol-2-one and the thiazole ring) are coplanar.

For **2a**, with the cyanoethylthio substituent on the thiazole ring, the molecule crystallizes in the triclinic system, space group *P* $\bar{1}$ . There is no relevant interatomic contacts shorter than 95% of the sum of the van der Waals radii between neighboring molecules indicating none or weak non-covalent intermolecular interactions. Contrariwise, for **2e** the presence of the thiocyanate group



**Scheme 5** Synthetic route towards TTF **4e**.

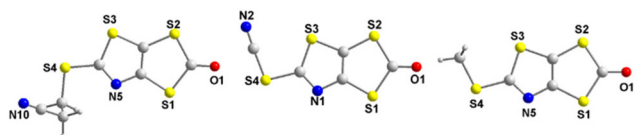


**Table 1** Redox potentials of the investigated TTFs in CH<sub>2</sub>Cl<sub>2</sub>, 0.1 M TBAPF<sub>6</sub> E in V vs. SCE

TTF	$E_{1/2}^1$ ( $\Delta E_p$ , mV)	$E_{1/2}^2$ ( $\Delta E_p$ , mV)
(MeS) <sub>4</sub> TTF	0.49 (60)	0.83 (60)
3a	0.63 (60)	0.97 (70)
3b	0.68/0.46	1.08/0.75
3c	0.74 (60)	1.12 (70)
3d	0.61 (60)	0.97 (60)
4a	0.56 (70)	0.91 (70)
4b	0.57 (80)	0.94 (80)
4c	0.59 (70)	0.94 (90)
4d	0.53 (60)	0.87 (60)
4e	0.58 (80)	0.89 (70)

**Table 2** Relevant interatomic distances in Å and angles (°) chalcogen bonding interactions

Distances (Å)	Type	RR%	Angles (°)
For 2e			
S <sub>2</sub> ⋯N <sub>2</sub> 3.051(2)	ChB	91.0	C <sub>1</sub> -S <sub>2</sub> ⋯N <sub>2</sub> 172.8(6) C <sub>5</sub> -N <sub>2</sub> ⋯S <sub>2</sub> 162.9(7)
S <sub>3</sub> ⋯N <sub>2</sub> 3.037(2)	ChB	90.6	C <sub>4</sub> -S <sub>3</sub> ⋯N <sub>2</sub> 168.6(9) C <sub>5</sub> -N <sub>2</sub> ⋯S <sub>3</sub> 132.3(1)
S <sub>1</sub> ⋯O <sub>1</sub> 3.168(2)	ChB	95.4	C <sub>1</sub> -S <sub>1</sub> ⋯O <sub>1</sub> 136.1(3) C <sub>1</sub> -O <sub>1</sub> ⋯S <sub>1</sub> 101.4(6)
S <sub>4</sub> ⋯O <sub>1</sub> 2.911(0)	ChB	87.6	C <sub>4</sub> -S <sub>4</sub> ⋯O <sub>1</sub> 162.8(8) C <sub>1</sub> -O <sub>1</sub> ⋯S <sub>4</sub> 163.7(5)
For 2f			
S <sub>2</sub> ⋯O <sub>1</sub> 2.862(2)	ChB	86.1	C <sub>2</sub> -S <sub>2</sub> ⋯O <sub>1</sub> 177.4(2) C <sub>2</sub> -O <sub>1</sub> ⋯S <sub>2</sub> 172.2(2)
S <sub>3</sub> ⋯O <sub>1</sub> 3.178(3)	ChB	95.4	C <sub>6</sub> -S <sub>3</sub> ⋯O <sub>1</sub> 166.3(1) C <sub>2</sub> -O <sub>1</sub> ⋯S <sub>3</sub> 110.6(2)
S <sub>1</sub> ⋯S <sub>4</sub> 3.395(2)	ChB	94.3	C <sub>2</sub> -S <sub>1</sub> ⋯S <sub>4</sub> 175.3(1) C <sub>6</sub> -S <sub>4</sub> ⋯S <sub>1</sub> 129.4(1)

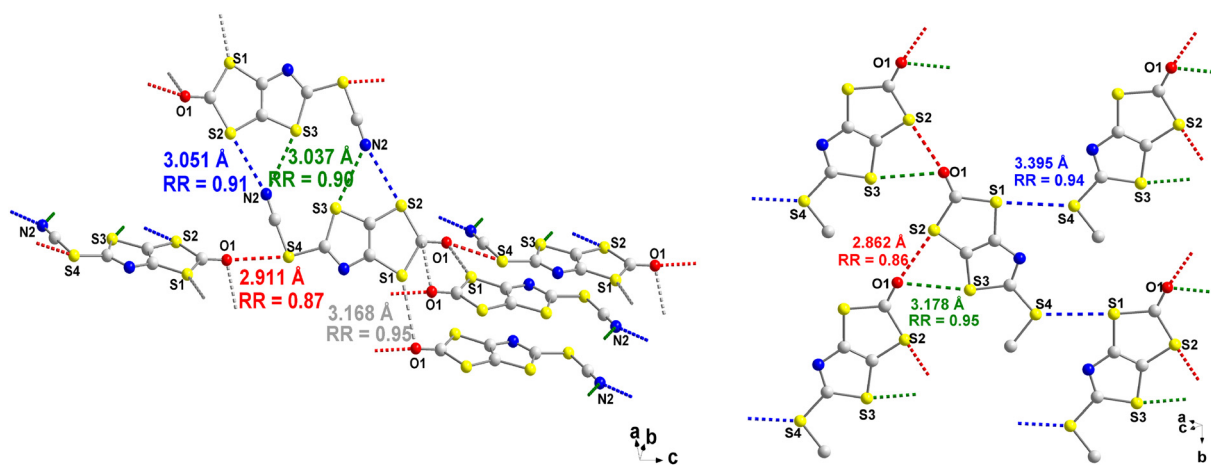
**Fig. 1** Molecular structures of 2a (left), 2e (middle) and 2f (right).

induces some intermolecular interactions. The crystal structure of 2e is solved in the monoclinic system, space group *C2/c*, with the molecule in general position. The molecules form “dimers” in the *ac* plane, stacking along the *b* axis. The “dimers” are related by an inversion center, and are held by chalcogen bonding between the nitrogen of the thiocyanate group (N2) as ChB acceptor of one molecule, and two opposite sulfur atoms (S3, S2) as ChB donors from the other molecule (Fig. 2 and Table 2). The C-S⋯N angles are in the range of 170°, and the S⋯N contacts are short with a 90% reduction ratio relative to the sum of the vdW radii (Fig. 2). There also exists strong S⋯O interactions, between the oxygen of dithiol-2-one and the sulfur of the thiocyanate group along the *c* axis, with a S⋯O distance of 2.911 Å indicating a reduction ratio of 87.6% compared to the sum of the vdW radii (3.32 Å). Weaker S⋯O interactions (3.168 Å, RR: 95%) are observed

along the *a* axis between the oxygen atom of the dithiol-2-one and the sulfur atom of the neighboring molecule.

For 2f, which crystallizes in the monoclinic system, space group *P2<sub>1</sub>/c*, a closer look at the structure shows the existence of chalcogen bonding interactions, involving the sulfur atoms of both heterocycles as ChB donors toward the O atom and the S-Me substituent as ChB acceptors, with a short S<sub>4</sub>⋯O<sub>1</sub> interatomic distance of 2.862 Å which corresponds to a reduction ratio of 86.1% relative to the van der Waals contact distance (3.32 Å). This chalcogen bonding interaction is reminiscent of what was previously observed with the iodo analogue 2c where a short S⋯O interatomic distance of 2.940 Å corresponding to a reduction ratio of 88.5% was observed.<sup>19,23</sup>

Concerning the neutral TTFs, crystals were obtained by slow evaporation of concentrated dichloromethane solution of the symmetrical TTF, 3d, and the three dissymmetrical TTF-R, 4a, 4b, 4e (R = SCH<sub>2</sub>CH<sub>2</sub>CN, H, and SCN respectively). The molecular structures of these TTFs are presented in Fig. 3. The crystal structure of 3d is solved in the monoclinic system, space group *P2<sub>1</sub>/a*, with the molecule in general position. The donor core is essentially planar with the two thioethyl substituents in the plane of the molecule. One TTF moiety is disordered on two positions (89:11) compatible with the presence of the two configurations, *Z* and *E*. The molecules organize into face-to-

**Fig. 2** Intermolecular short contacts with the indicated reduction ratio relative to the sum of the vdW radii of the atoms for 2e (left) and 2f with hydrogen atoms omitted for clarity (right).



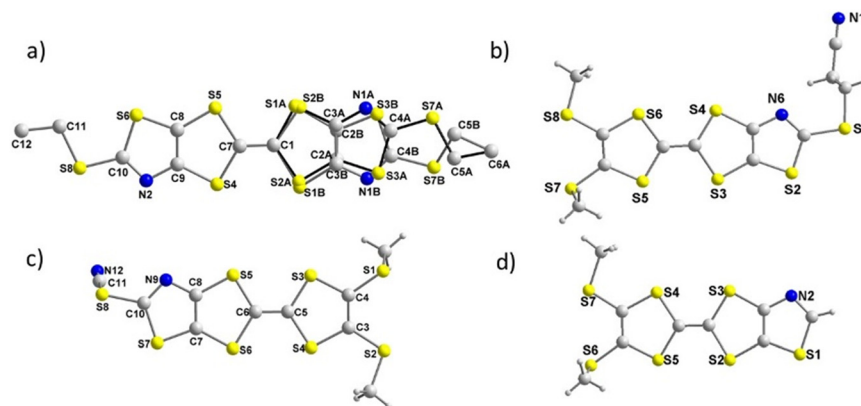


Fig. 3 Molecular structures of symmetrical TTF 3d (a) and dissymmetrical TTFs 4a (b) 4e (c) and 4b (d).

face inversion-centered dimers with a plane-to-plane distance of 3.50 Å, slightly shorter than the S⋯S van der Waals contact distance (Fig. S1†). The dimers adopt a herringbone organization (Fig. S1b†), reminiscent of the kappa-type phases observed in BEDT-TTF salts.<sup>24</sup> No other short intermolecular contacts are identified.

The crystal structure of the dissymmetrically substituted TTFs are solved in the triclinic system, space group  $P\bar{1}$ . Analysis of the structure reveals some similarities for the three investigated TTFs, such as a planar TTF core with one thiomethyl group in the plane of the TTF while the other one points above the plane. Concerning the TTF 4a, the cyanoethyl group is located below the plane (Fig. 3). A closer look at the interatomic distances in 4a indicates that no contact shorter than the sum of the van der Waals radii can be observed between adjacent molecules. The molecules organize through  $\pi$ - $\pi$  stacking into uniform stacks running along  $a$  axis with a plane-to-plane distance of 3.60 Å, *i.e.* at van der Waals contact distance (Fig. S2†).

Contrariwise, for 4b, as shown in Fig. 4, two main short interatomic distances can be observed between adjacent TTFs. These short contacts involve the hydrogen of the methyl group of one TTF as HB donor with the nitrogen atom (N2) of the second TTF as HB acceptor, with a H⋯N distance of 2.541 Å, and the hydrogen atom of the thiazole ring on one TTF with the sulfur (S7) atom of another TTF, with a H⋯S distance of 2.843 Å (Fig. 4). Both distances are shorter than the van der Waals contact distances which amount to 2.75 Å for H⋯N (1.2 + 1.55) and to 3 Å for H⋯S (1.2 + 1.8) which leads to a reduction ratio of 92.4% for H⋯N and 94.7% for S⋯H. Moreover the C-H⋯N and C-H⋯S angles amount to 176.3(2)° and 160.4(1)° respectively indicating the

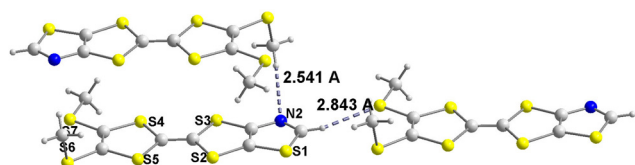


Fig. 4 Hydrogen bonding interactions in TTF 4b.

existence of hydrogen bonding interaction (HB) between neighboring TTFs. Concerning TTF 4e, no intermolecular interactions through chalcogen bonding involving the sulfur atom of the thiocyanate group is observed, in contrast to the strong ones observed for 2e. Molecules are organized into strongly dimerized stacks, with a plane-to-plane distance of 3.50 Å within face-to-face dimers and a longer 4.00 Å plane-to-plane-distance between dimers (Fig. S3†). No other characteristic intermolecular short contacts are identified.

### Charge transfer complexes

The oxidation potentials of all the obtained TTFs are too high for using the TCNQ as oxidizing agent. Indeed, TCNQ is reduced at 0.18 V *vs.* SCE and all the TTFs 3 and 4 are oxidized above 0.53 V *vs.* SCE and with such potential difference no redox reaction is expected between the TCNQ and the TTFs. In order to generate a charge transfer complex, we decided to use a stronger electron acceptor such as TCNQF<sub>4</sub> which is reduced at 0.53 V *vs.* SCE. Crystals were obtained when mixing 4b and 4c with TCNQF<sub>4</sub>. For the complex obtained with 4c, it crystallizes in the triclinic system, space group  $P\bar{1}$ , with one TTF in general position in the unit cell and the TCNQF<sub>4</sub> on an inversion center. The crystal structure determination indicates a stoichiometry of two donors for one TCNQF<sub>4</sub>, (4c)<sub>2</sub>(TCNQF<sub>4</sub>). Within this complex, dyads of TTFs alternate with TCNQF<sub>4</sub> in a  $-(D_2-A)_x-$  motif.<sup>25</sup> Within the donor dyad the TTF are organized head to tail with a bond over ring overlap (Fig. 5). Several short intermolecular contacts can be observed within the  $ac$  plane: i) I⋯S2 between the iodo atom of one TTF and the sulfur atom of the thiomethyl group of a neighboring TTF (3.404 Å) and ii) F⋯S between a fluorine atom of one TCNQF<sub>4</sub> and the sulfur atom within a dithiole ring of the neighboring TTF (3.122 Å). The bond distances, reduction ratio and angles are collected in Table 3. Chalcogen interactions are also found: i) short S⋯S distances between the sulfur atom of one TTF and the sulfur atom of the neighboring TTF (3.279 Å) and ii) S⋯N between the nitrogen atom of one TCNQF<sub>4</sub> and the sulfur atom of the neighboring TTF (3.019 Å) (Fig. 5).



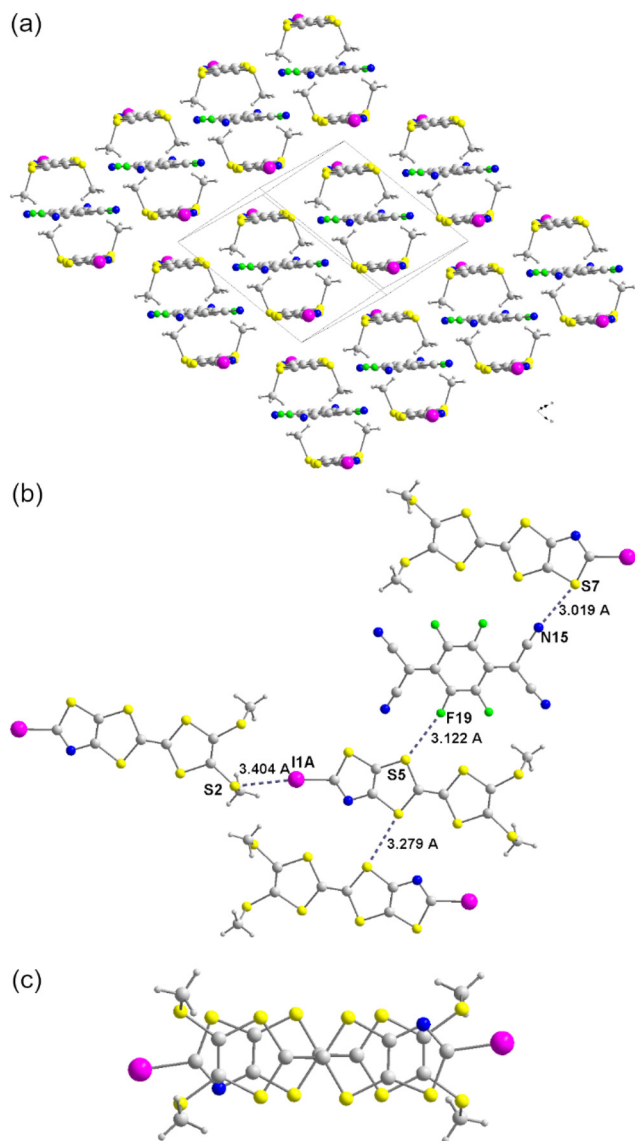


Fig. 5 Projection view of  $(4c)_2(TCNQF_4)$  complex along the long axis of TTF and  $TCNQF_4$  showing the  $-(D_2-A)_x-$  motif (a). View of the short contacts observed in the organization of  $(4c)_2(TCNQF_4)$  along the  $ac$  plane (b) and view of the TTF dyad overlap (c).

**Table 3** Relevant interatomic distances (Å), reduction ratio (RR) and angles ( $^\circ$ ) for the halogen bonding and chalcogen interactions in  $(4c)_2(TCNQF_4)$ . The van der Waals contact distances amount to  $S \cdots I$ : 3.78 Å,  $S \cdots S$ : 3.60 Å,  $S \cdots F$ : 3.27 Å,  $S \cdots N$ : 3.35 Å

	Distances (Å)	RR	Angles ( $^\circ$ )
$(4c)_2(TCNQF_4)$	$S_6 \cdots S_6$ 3.279	91%	$C-S_6 \cdots S_6$ 164.7
	$S_7 \cdots N_{15}$ 3.019	95%	$C-S_7 \cdots N_{15}$ 163.4
	$S_2 \cdots I_1$ 3.404	90%	$C-I_1 \cdots S_2$ 172.7
	$S_5 \cdots F_{19}$ 3.122	95%	$C-F_{19} \cdots S_5$ 166.5

The charge transfer complex obtained with **4b** crystallizes in the triclinic system, space group  $P\bar{1}$ . Crystal structure determination indicates a stoichiometry of one donor for one  $TCNQF_4$ ,  $(4b)(TCNQF_4)$ , with **4b** and  $TCNQF_4$  organized in

segregated stacks (Fig. 6). The thiazole ring of the TTF is disordered on two positions (86:14). Within the donor stacks, the dissymmetrical TTFs are organized head to tail with the thiazole ring of one TTF over the bisthiomethyl substituents of the dithiole ring of the neighboring TTF. The stacks are not uniform as shown by the two distances measured between the planes of the TTF, 3.575 Å and 3.355 Å indicating that the **4b** are actually dimerized along the stacking axis. Similarly the  $TCNQF_4$  form dimerized stacks with a short interplanar distance within the dimer (3.086 Å) and an almost eclipsed overlap. A lateral slip exist between neighboring dimers with a longer interplanar distance of 3.399 Å. No specific hydrogen, halogen or chalcogen interactions can be observed within this complex.

In order to determine the degree of charge transfer within  $(4b)(TCNQF_4)$  and  $(4c)_2(TCNQF_4)$  complexes, we analyzed the bond lengths of the  $TCNQF_4$  skeleton. For that purpose we collected in Table 4 the bond lengths of the neutral  $TCNQF_4$  and the bond length of the  $TCNQF_4$  involved in each complex. As can be seen, the acceptor bond lengths within our complex are different than those reported for the neutral  $TCNQF_4$  indicating that these complexes are not neutral. The charge of  $TCNQF_4$  can be estimated by the Kistenmacher relationship first established for TCNQ salts by Kistenmacher *et al.*,<sup>26</sup> and adapted to  $TCNQF_4$  by Miyasaka *et al.*<sup>27</sup> It is estimated from the bond lengths  $b$ ,  $c$  and  $d$  of the acceptor through the equation  $\rho_{TCNQF_4} = A[c/(b + d)] + B$ , where  $A = -46.729$  and  $B = 22.308$ .

From this equation we found a charge of  $-0.78$  on the  $TCNQF_4$  for  $(4c)_2(TCNQF_4)$  and a charge of  $-0.90$  on the  $TCNQF_4$  for  $(4b)(TCNQF_4)$  confirming that both complexes are charge transfer salts. Based on the nitrile stretching absorption band of  $TCNQF_4$ , it is also possible to infer the degree of charge transfer in those  $TCNQF_4$  complexes. The value obtained for the neutral  $TCNQF_4$  is observed at  $\nu_{CN}$  2228  $cm^{-1}$  and the value for the radical anion  $TCNQF_4^{\cdot-}$  at  $\nu_{CN}$  2190  $cm^{-1}$ .<sup>29</sup> The value obtained for the two complexes amounts to 2189  $cm^{-1}$  which is close to that observed for the radical anion  $TCNQF_4^{\cdot-}$ . This is consistent with the values determined through the bond distances analysis in  $TCNQF_4$ . Moreover if we compare the bond length of the neutral **4b** (see above) with the one of the TTF within  $(4b)(TCNQF_4)$ , we can see that the central  $C=C$  bond is lengthened in the charge transfer salt in accordance with the presence of an oxidized TTF (1.344 Å in **4b** and 1.385 Å in  $(4b)(TCNQF_4)$ ). Thus this complex is a fully ionic complex. Resistivity measurements were performed on  $(4b)(TCNQF_4)$  and the room temperature resistivity was found to be  $1.5 \times 10^4 \Omega cm$ . This high resistivity is essentially a consequence of the strong dimerization within the TTF stacks.

### Electrostatic potential surface study

Electrostatic potential (ESP) surface calculations have been carried out on the DFT-optimized geometry of the precursors that have been crystallographically characterized, namely **2e**,



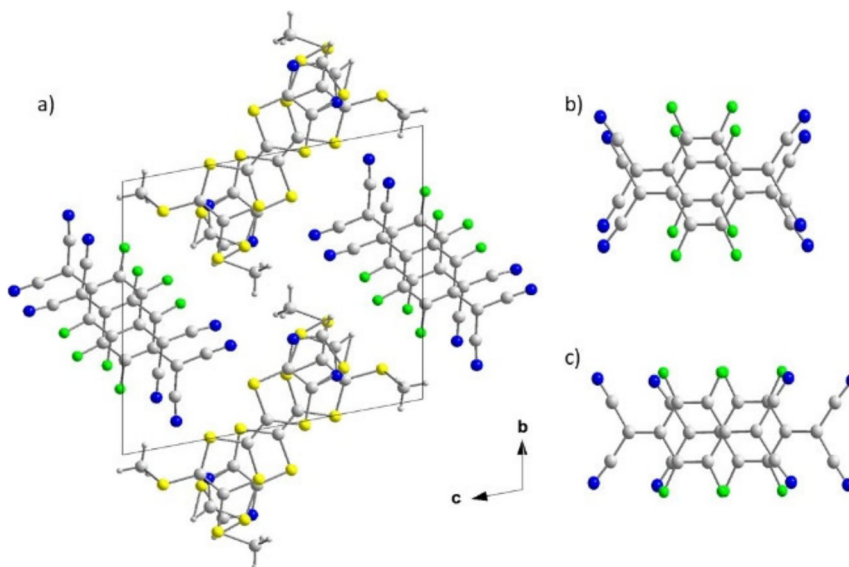


Fig. 6 View of the unit cell of (4b)(TCNQF<sub>4</sub>) along the *bc* plane (a) and view of the TCNQF<sub>4</sub> intra-dimer (b) and inter-dimer (c) overlap patterns in the acceptor stacks.

Table 4 TCNQF<sub>4</sub> bond lengths in Å

	<i>a</i>	<i>b</i>	<i>c</i>	<i>d</i>	$\rho_{\text{TCNQF}_4}$ (calc)
TCNQF <sub>4</sub> <sup>0</sup>	1.334	1.437	1.372	1.437	0
(4c) <sub>2</sub> (TCNQF <sub>4</sub> )	1.352	1.419	1.409	1.432	-0.786
(4b)(TCNQF <sub>4</sub> )	1.356	1.414	1.410	1.425	-0.90
(TBA)(TCNQF <sub>4</sub> ) <sup>28</sup>	1.357	1.417	1.418	1.425	-1

and **2f** as well as on three TTFs, **4b**, **4c** and **4e** (R = H, I, SCN). These calculations were performed in order to rationalize the interactions taking place in the crystal.

As shown in Fig. 7, for **2e** and **2f** the positive extremum of the ESP surface is found close to the carbon atom connecting the thiazole and the dithiole rings (+40.2 kcal mol<sup>-1</sup> for **2e** and +32.0 for **2f**) and to a lesser extent on the side of the sulfur atom of the S-CN fragment (+33.0 kcal mol<sup>-1</sup> for **2e**). The location of this positive charge on the sulfur atom, on the opposite side of the thiazole ring, indicates that the

thiazole ring exerts a stronger electron withdrawing effect than the cyano group. For **2f** interestingly, a non-negligible positive ESP is also found on the hydrogen atoms of the thiomethyl substituent. The most negative extremum is -26.3 kcal mol<sup>-1</sup> and is located on the nitrogen atom of the thiocyanate group and to a lesser extent on the oxygen atom of the dithiol-2-one ring (-24.0 kcal per mole) for **2e** while for **2f** the most negative extremum is -29.2 kcal mol<sup>-1</sup> and is located on the oxygen atom. This calculated charge repartition is in good agreement with the organization of the

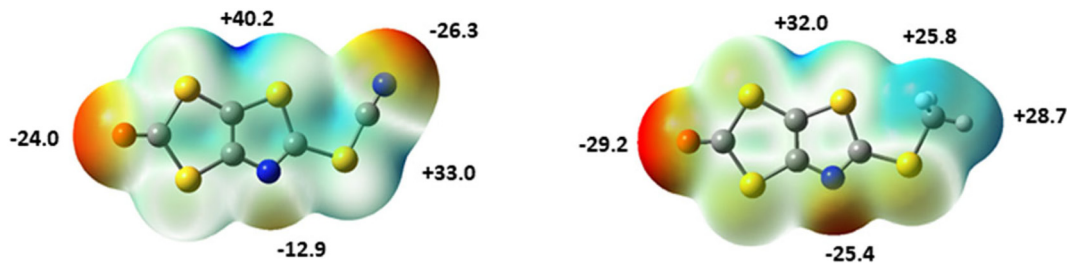


Fig. 7 Molecular electrostatic potential surfaces mapped at 0.001 e<sup>-</sup> au<sup>-3</sup> isodensity surface for (left) **2e** and (right) **2f**. The common color scale ranges from -28 kcal mol<sup>-1</sup> (red) to +40 kcal mol<sup>-1</sup> (blue).





molecules **2e** and **2f** in the solid state where predominant ChB interactions ( $S\cdots O$ ) are observed together with  $S\cdots N$  interactions for **2e**.

The hydrogen and halogen bond donor abilities of the TTF derivatives can also be estimated *via* the calculation of the ESP and especially its magnitude at the  $\sigma$ -holes. These calculations have been performed on **4b**, **4c** and **4e** in order to analyze the impact of the R group. As shown in Fig. 8, the most depleted charged area is associated with the  $\sigma$ -hole on the iodine atom of **4c** and on the  $\sigma$ -hole of the hydrogen atom of **4b**. Both TTF exhibit also a charge depletion on the hydrogen atom of the thiomethyl substituents as shown for **4b** in Fig. 8. For **4b** and **4c**, the most negative extremum, is located on the nitrogen atom of the thiazole ring and to a lesser extent on the sulfur atoms of the thiomethyl substituent ( $-23.7$  kcal mol $^{-1}$  for **4b**). This charge distribution is consistent with the obtained solid-state arrangement, and the preferred HB interactions observed for **4b** (Fig. 4) but not for **4e**.

The electrostatic surface potential at the iodine atom of **4c** is found to logically increase with the charge of molecule from  $+32.0$  to  $+82.8$  kcal mol $^{-1}$  for the neutral, radical cation respectively (blue dot on iodine in Fig. 8 and 9). Similarly on **4b** the charge depletion on the hydrogen atom is increased on the **4b** cation radical. Another interesting observation is that the negative charge at the nitrogen atom of the thiocyanate of **4e** is reversed (from  $-36.4$  to  $+13.1$  kcal mol $^{-1}$ ) as the molecule is oxidized. As a charge of  $+0.5$  is borne out by each TTF in the complex  $(4c)_2(\text{TCNQF}_4)$  it is not possible to draw the corresponding ESP surface. However the fact that intermolecular interactions exist between the iodine atom of one  $4c^{+0.5}$  and the sulfur atom of the neighboring  $4c^{+0.5}$  molecule is consistent with the charge distribution.

## Conclusions

Within this work, we have designed TTF precursors with both, hydrogen, halogen and chalcogen bonding, donor and acceptor sites thanks to an original transformation of the *N*-*t*Bu-1,3-thiazoline-2-thione fused dithiol-2-one. For that purpose, we prepared the precursors with a dithiole-2-one ring that serves as a TTF building block substituted either with cyanoethyl groups, iodine atoms, thiocyanate-groups or simply an H atom. Symmetrically and dissymmetrically substituted TTFs able to form hydrogen, halogen and

chalcogen bonds depending on the substitution pattern have been synthesized. Symmetrical TTFs were prepared by a homocoupling of the dithiole-2-one precursors, while the dissymmetrical TTFs were formed, in higher yields, through a heterocoupling. All the synthesized TTFs were studied by cyclic voltammetry, and the effect of the different functional groups on the redox potentials were determined. Structural investigations of the precursors and the TTFs highlight some differences in the intermolecular interactions which could be corroborated with ESP calculations. Charge transfer salts using TCNQF $_4$  as an acceptor were also prepared and X-ray diffraction studies of these salts,  $(4c)_2(\text{TCNQF}_4)$  and  $(4b)(\text{TCNQF}_4)$ , show different stacking mode. Investigation of the bond length allowed us to determine that  $(4b)(\text{TCNQF}_4)$ , is fully ionic while a partial degree of charge transfer was found in  $(4c)_2(\text{TCNQF}_4)$ . In the latter salt strong non-covalent interactions between the donor molecules themselves and between the donor and acceptor moieties have been evidenced. We have identified and characterized intermolecular non-covalent interactions through analysis of intermolecular angles and distances in the crystal structure that are significantly shorter than the sum of the van der Waals radii. This has been supported by calculations of electrostatic surface potential on the DFT optimized structure of the molecules. To further characterize and quantify non-covalent bonds in single crystals, application of Bader's theory of atoms in molecules (AIM) $^{30}$  is planned for our subsequent works.

## Experimental section

### General information

All commercial chemicals were used without further purification. The solvents were purified and dried by standard methods. NMR spectra were obtained in CDCl $_3$  unless indicated otherwise. Chemical shifts are reported in ppm,  $^1\text{H}$  NMR spectra were referenced to residual CHCl $_3$  (7.26 ppm) and  $^{13}\text{C}$  NMR spectra were referenced to CHCl $_3$  (77.2 ppm). Compounds **2b** and **2e** were prepared in degassed 99% DMSO. Melting points were measured on a Kofler hot-stage apparatus and are uncorrected. Mass spectra were recorded at the Centre Régional de Mesures Physiques de l'Ouest, Rennes. Elemental analyses were performed at the Service de Microanalyse, Gif sur Yvette. Cyclic voltammetry were carried out on a  $10^{-3}$  M solution in CH $_2$ Cl $_2$ , containing

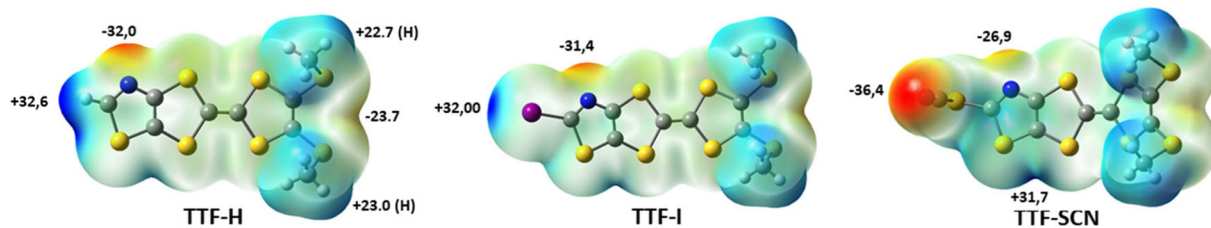


Fig. 8 Molecular electrostatic potential surfaces mapped at  $0.001$  e $^{-}$  au $^{-3}$  isodensity surface for **4b** (TTF-H), **4c** (TTF-I), and **4e** (TTF-SCN). The common color scale ranges from  $-37$  kcal mol $^{-1}$  (red) to  $+32.6$  kcal mol $^{-1}$  (blue).



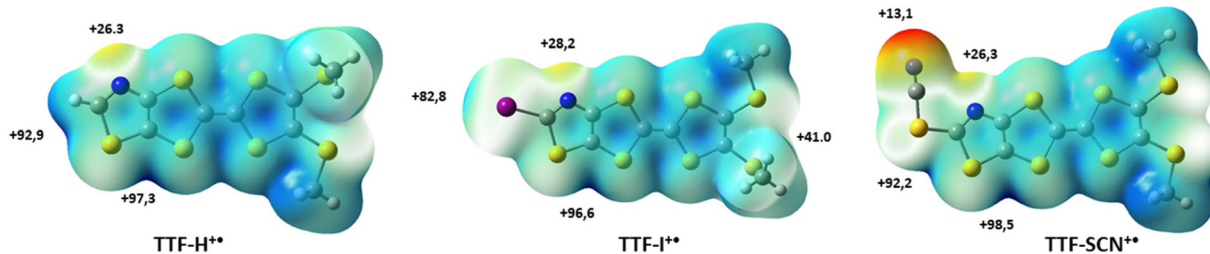


Fig. 9 Molecular electrostatic potential surfaces mapped at  $0.001 \text{ e}^- \text{ au}^{-3}$  isodensity surface for the cation radical state of  $4b^{+\bullet}$  (TTF- $H^{+\bullet}$ ),  $4c^{+\bullet}$  (TTF- $I^{+\bullet}$ ) and  $4e^{+\bullet}$  (TTF- $SCN^{+\bullet}$ ). The common color scale ranges from  $13.13 \text{ kcal mol}^{-1}$  (red) to  $+98.5 \text{ kcal mol}^{-1}$  (blue).

0.1 M  $n\text{Bu}_4\text{NPF}_6$  as supporting electrolyte. Voltammograms were recorded at  $0.1 \text{ V s}^{-1}$  on a platinum electrode and the potentials were measured *versus* the saturated calomel electrode (SCE). The starting derivative **1** (ref. 17) as well as **2c**<sup>19</sup> and **2d**<sup>17</sup> were prepared according to the procedure previously described.

### 3-((2-Oxo-[1,3]dithiolo[4,5-*d*]thiazol-5-yl)thio)propanenitrile **2a**

Under inert atmosphere, to a solution of **1** (600 mg; 2.28 mmol) in 8 mL of degassed DMF, 3-bromopropionitrile (1.52 mL; 18.16 mmol) was added. The reaction mixture was stirred at  $70 \text{ }^\circ\text{C}$  for 48 hours. The reaction was quenched with 200 mL of water and the product was extracted with  $\text{CH}_2\text{Cl}_2$ . The organic phase was washed 10 times with water and dried over  $\text{MgSO}_4$ . The concentrated solution was purified by flash chromatography using a mixture of petroleum ether and  $\text{CH}_2\text{Cl}_2$  starting from 0 to 15% of  $\text{CH}_2\text{Cl}_2$  to afford **2a** as orange powder in 63% yield ( $m = 375 \text{ mg}$ ). Crystals of sufficient quality for X-ray diffraction were obtained by slow evaporation of a concentrated dichloromethane solution.  $R_f = 0.37$ , ( $\text{SiO}_2$ ,  $\text{CH}_2\text{Cl}_2$ );  $\text{mp} = 103 \text{ }^\circ\text{C}$ ;  $^1\text{H NMR}$  (300 MHz)  $\delta$  3.50 (t,  $^3J = 6.9 \text{ Hz}$ , 2H), 2.95 (t,  $^3J = 6.9 \text{ Hz}$ , 2H);  $^{13}\text{C NMR}$  (75 MHz)  $\delta$  190.0 (C=O), 164.3 (C=N), 142.2 (C=C), 117.5 (C=C), 117.0 (C=N), 30.0 (S- $\text{CH}_2$ ), 18.6 (C $\text{H}_2$ CN); HRMS (ASAP) calcd for  $[\text{M}]^{+\bullet}$ : 259.9201; found: 259.9199; anal. calcd for  $\text{C}_7\text{H}_4\text{N}_2\text{OS}_4$ : C, 32.29; H, 1.55; N, 10.76; S, 49.25; found: C, 32.17; H, 1.80; N, 10.28; S, 49.26.

### [1,3]Dithiolo[4,5-*d*]thiazol-2-one **2b**

Under inert atmosphere, to a solution of **1** (300 mg; 1.14 mmol) in 4 mL of degassed DMSO, 3-bromopropionitrile (0.76 mL; 9.04 mmol) was added. The reaction mixture was stirred at  $55 \text{ }^\circ\text{C}$  for 48 hours. The reaction was quenched with 200 mL of water, and the product was extracted with  $\text{CH}_2\text{Cl}_2$ . The organic phase was washed 10 times with water and dried over  $\text{MgSO}_4$ . The concentrated solution was purified by flash chromatography using a mixture of petroleum ether and  $\text{CH}_2\text{Cl}_2$  starting from 0 to 15% of  $\text{CH}_2\text{Cl}_2$  to afford **2b** as white powder in 55% yield ( $m = 110 \text{ mg}$ );  $R_f = 0.56$ , ( $\text{SiO}_2$ ,  $\text{CH}_2\text{Cl}_2$ );  $\text{mp} = 120 \text{ }^\circ\text{C}$ ;  $^1\text{H NMR}$  (300 MHz)  $\delta$  8.97 (s, 1H);  $^{13}\text{C NMR}$  (75 MHz)  $\delta$  190.7 (C=O), 153.5 (N=C-H), 143.9 (C=C), 118.1 (C=C); HRMS (ESI) calcd for  $\text{C}_4\text{H}_2\text{NOS}_3^+$ : 175.9293. Found: 175.9294.<sup>19</sup>

### 5-Thiocyanato-[1,3]dithiolo[4,5-*d*]thiazol-2-one **2e**

Under inert atmosphere, to a solution of **1** (300 mg, 1.14 mmol) in 3 mL of DMSO, cyanogen bromide (0.97 g, 9.1 mmol), was added. The reaction mixture was let to stir at  $55 \text{ }^\circ\text{C}$  for 16 hours. The reaction was then quenched with water (200 mL), the product was then extracted with  $\text{CH}_2\text{Cl}_2$  and the organic phase was washed with water and then dried over  $\text{MgSO}_4$ . The solvent was evaporated under vacuum and the crude product was purified by flash chromatography using  $\text{CH}_2\text{Cl}_2$ /petroleum ether (40:60) as eluent giving compound **2e** as a white powder. Yield = 50% (133 mg);  $R_f = 0.52$ , ( $\text{SiO}_2$ ,  $\text{CH}_2\text{Cl}_2$ );  $\text{mp} = 132 \text{ }^\circ\text{C}$ .  $^{13}\text{C NMR}$  (75 MHz)  $\delta$  188.3 (C=O), 150.0 (C-S-CN), 144.5 (C=C), 123.5 (C=N), 106.4 (C=C). HRMS (ASAP) calcd for  $\text{C}_5\text{HN}_2\text{OS}_4^+$ : 232.89662, found: 232.8969; anal. calcd for  $\text{C}_5\text{N}_2\text{OS}_4$ : C, 25.85; N, 12.06. Found: C, 25.87; N, 12.34.

### TTF **3a**

Under inert atmosphere, a solution of **2a** (100 mg; 0.38 mmol) in 5 mL of distilled triethylphosphite was stirred at  $120 \text{ }^\circ\text{C}$  for 5 hours. The solvent was evaporated *in vacuo* and the residue was extracted with  $\text{CH}_2\text{Cl}_2$ . The organic phase was washed with water and dried over  $\text{MgSO}_4$ . The concentrated solution was purified by chromatography using  $\text{CH}_2\text{Cl}_2$  as eluent to afford the expected TTF as an orange powder. Yield = 22% ( $m = 21 \text{ mg}$ );  $R_f = 0.17$  ( $\text{SiO}_2$ ,  $\text{CH}_2\text{Cl}_2$ );  $\text{mp} = 220 \text{ }^\circ\text{C}$ ;  $^1\text{H NMR}$  (400 MHz)  $\delta$  3.46 (t,  $^3J = 7.1 \text{ Hz}$ , 4H), 2.93 (t,  $^3J = 7.1 \text{ Hz}$ , 4H). HRMS (ASAP) calcd for  $[\text{C}_{14}\text{H}_8\text{N}_4\text{S}_8 + \text{H}]^+$ : 438.85875; found: 488.8590.

### TTF **3b**

Under inert atmosphere, a solution of **2b** (60 mg; 0.34 mmol) in 5 mL of distilled triethylphosphite was stirred at  $120 \text{ }^\circ\text{C}$  for 2 hours. An orange precipitate was observed. The precipitate was filtered off and washed with methanol to afford **3b** as a brown powder. Yield = 24% ( $m = 13 \text{ mg}$ );  $R_f = 0.33$  ( $\text{SiO}_2$ ,  $\text{CH}_2\text{Cl}_2$ );  $\text{mp} = >260 \text{ }^\circ\text{C}$ ;  $^1\text{H NMR}$  (400 MHz, DMSO)  $\delta$  (ppm) = 9.10 (s, 2H);  $^{13}\text{C NMR}$  (75 MHz, DMSO)  $\delta$  (ppm) = 159.8 (C $\text{H}$ ), 147.5 (C=C), 123.7 (C=C), 123.4 (C=C). HRMS (ASAP) calcd for  $[\text{M} + \text{H}]^+$   $\text{C}_8\text{H}_3\text{N}_2\text{S}_6$ : 318.8615; found: 318.8617; anal. calcd for  $\text{C}_8\text{H}_2\text{N}_2\text{S}_6 \cdot \text{CH}_3\text{OH}$ : C, 30.84; H, 1.73; N, 7.99. Found: C, 30.98; H, 1.41; N, 7.39.



**TTF 3c**

Under inert atmosphere, a solution of **2c** (60 mg; 0.19 mmol) in 5 mL of distilled triethylphosphite was stirred at 120 °C for 2 hours. The solvent was evaporated *in vacuo* and the residue was extracted with CH<sub>2</sub>Cl<sub>2</sub>. The organic phase was washed with water and dried over MgSO<sub>4</sub>. The concentrated solution was purified by chromatography using CH<sub>2</sub>Cl<sub>2</sub> as eluent to afford **3c** as an orange powder. Yield = 23% (*m* = 13 mg); Mp > 240 °C; HRMS (ESI) calcd for [C<sub>8</sub>N<sub>2</sub>I<sub>2</sub>S<sub>8</sub><sup>+</sup>]: 569.64698, found: 569.6474.

**TTF 3d**

In a two necked flask purged with argon, the bicyclic derivative **2d** (100 mg, 0.42 mmol) was solubilized in 3 mL of degassed chlorobenzene, 0.5 mL of triethylphosphite was then added to the solution followed by 3 hours at reflux. The solvent was then evaporated and the product was purified using flash chromatography (eluent: CH<sub>2</sub>Cl<sub>2</sub>/petroleum ether; 20:80), after evaporation of the solvent the product was obtained as an orange powder which was recrystallized in CH<sub>2</sub>Cl<sub>2</sub> to afford bright orange needles. Yield = 27% (25 mg); Rf = 0.52, (SiO<sub>2</sub>, CH<sub>2</sub>Cl<sub>2</sub>); mp = 205 °C; <sup>1</sup>H NMR (300 MHz) δ 3.17 (q, <sup>3</sup>J = 7.3 Hz, 4H), 1.41 (t, <sup>3</sup>J = 7.3 Hz, 6H); HRMS (ESI) calcd for [A<sup>+</sup>] C<sub>12</sub>H<sub>10</sub>N<sub>2</sub>S<sub>8</sub>: 437.86042, found: 437.8603; anal. calcd for C<sub>12</sub>H<sub>10</sub>N<sub>2</sub>S<sub>8</sub>: C, 32.85; H, 2.30; N, 6.39. Found: C, 32.62; H, 2.17; N, 6.32.

**General synthesis of TTFs 4a–d through the heterocoupling**

Under inert atmosphere, a solution of **2a–c** (0.22 mmol, **2a** 57 mg, **2b** 38 mg, **2c** 66 mg) and **3** (50 mg; 0.22 mmol) in 5 mL of distilled triethylphosphite was stirred at 120 °C for 2 hours. The solvent was evaporated *in vacuo* and the residue was extracted with CH<sub>2</sub>Cl<sub>2</sub>. The organic phase was washed with water and dried over MgSO<sub>4</sub>.

**TTF 4a**

The reaction mixture was purified by chromatography using CH<sub>2</sub>Cl<sub>2</sub> as eluent to afford the TTF as an orange powder. Crystals of sufficient quality for X-ray diffraction were obtained by slow evaporation of a concentrated dichloromethane solution. Yield = 24% (*m* = 23 mg); Rf = 0.67 (SiO<sub>2</sub>, CH<sub>2</sub>Cl<sub>2</sub>); mp = 173 °C; <sup>1</sup>H NMR (300 MHz, CD<sub>2</sub>Cl<sub>2</sub>) δ 3.40 (t, <sup>3</sup>J = 6.9 Hz, 2H), 2.89 (t, <sup>3</sup>J = 7.0 Hz, 2H), 2.44 (s, SCH<sub>3</sub>), 2.43 (s, SCH<sub>3</sub>); <sup>13</sup>C NMR (75 MHz, CD<sub>2</sub>Cl<sub>2</sub>) δ 163.8 (C=C), 148.1 (C=N), 127.7 (C=C), 127.2 (C=C), 117.4 (CN), 112.4 (C=C), 30.5 (SCH<sub>2</sub>), 18.8 (C-CH<sub>2</sub>), 18.3 (CH<sub>3</sub>); HRMS (ASAP) calcd for [C<sub>12</sub>H<sub>10</sub>N<sub>2</sub>S<sub>8</sub>]<sup>+</sup>: 437.86097. Found: 437.86042; anal. calcd for C<sub>12</sub>H<sub>10</sub>N<sub>2</sub>S<sub>8</sub>·0.5CH<sub>2</sub>Cl<sub>2</sub>: C, 31.20; H, 2.30; N, 5.82. Found: C, 30.82; H, 2.00; N, 6.00.

**TTF 4b**

The concentrated solution was purified by chromatography using CH<sub>2</sub>Cl<sub>2</sub> as eluent to afford **4b** as a red powder. Crystals of sufficient quality for X-ray diffraction were obtained by

slow evaporation of a concentrated dichloromethane solution. Yield = 38% (*m* = 30 mg); Rf = 0.6 (SiO<sub>2</sub>, CH<sub>2</sub>Cl<sub>2</sub>); mp = 125 °C; <sup>1</sup>H NMR (400 MHz) δ 8.68 (s, 1H), 2.44 (s, SCH<sub>3</sub>), 2.43 (s, SCH<sub>3</sub>); <sup>13</sup>C NMR (75 MHz) δ 154.8 (C-H), 150.6 (C=C), 128.1 (C=C), 127.1 (C=C), 122.1 (C=C), 114.2 (C=C), 19.2 (CH<sub>3</sub>); HRMS (ASAP) calcd for [C<sub>9</sub>H<sub>7</sub>NS<sub>7</sub> + H]<sup>+</sup>: 353.86963. Found: 353.8693; anal. calcd for C<sub>9</sub>H<sub>7</sub>NS<sub>7</sub>: C, 30.57; H, 2.00; N, 3.96. Found: C, 30.08; H, 1.82; N, 3.80.

**TTF 4c**

The concentrated solution was purified by chromatography using CH<sub>2</sub>Cl<sub>2</sub>/petroleum ether (60/40) as eluent to afford **4c** as a red powder. Yield = 19% (*m* = 20 mg); Rf = 0.83 (SiO<sub>2</sub>, CH<sub>2</sub>Cl<sub>2</sub>); mp = 147 °C; <sup>1</sup>H NMR (300 MHz) δ 2.44 (s, SCH<sub>3</sub>), 2.43 (s, SCH<sub>3</sub>); <sup>13</sup>C NMR (75 MHz) δ 155.2 (C-I), 149.6 (C=N), 128.7 (C=C), 128.2 (C=C), 127.0 (C=C), 126.1 (C=C), 100.7 (C=C), 19.3 (SCH<sub>3</sub>); HRMS (ASAP) calcd for [C<sub>9</sub>H<sub>6</sub>NIS<sub>7</sub>]<sup>+</sup>: 478.75845; found: 478.7588.

**TTF 4d**

Under inert atmosphere, a solution of **1** (58 mg; 0.22 mmol) and **3** (50 mg; 0.22 mmol) in 10 mL of distilled triethylphosphite was stirred at 120 °C for 2 hours. The solvent was evaporated *in vacuo* and the residue was extracted with CH<sub>2</sub>Cl<sub>2</sub>. The organic phase was washed with water and dried over MgSO<sub>4</sub>. The concentrated solution was purified by chromatography using CH<sub>2</sub>Cl<sub>2</sub>/petroleum ether (90/10) as eluent to afford **4d** as a red powder. Yield = 46% (*m* = 42 mg); Rf = 0.73 (SiO<sub>2</sub>, CH<sub>2</sub>Cl<sub>2</sub>); mp = 100 °C; <sup>1</sup>H NMR (400 MHz) δ 3.17 (q, <sup>3</sup>J = 7.3 Hz, CH<sub>2</sub>CH<sub>3</sub>), 2.44 (s, 6H, SCH<sub>3</sub>), 1.40 (t, <sup>3</sup>J = 7.3 Hz, CH<sub>2</sub>CH<sub>3</sub>); <sup>13</sup>C NMR (75 MHz) δ 166.9 (C=C), 148.3 (CSEt), 128.1 (C=C), 127.3 (C=C), 120.4 (C=C), 113.7 (C=C), 30.2 (CH<sub>2</sub>), 19.4 (SCH<sub>3</sub>), 14.7(CH<sub>2</sub>CH<sub>3</sub>); HRMS (ESI) calcd for [C<sub>11</sub>H<sub>11</sub>NS<sub>8</sub>Na]<sup>+</sup>: 435.85494; found: 435.8550; anal. calcd for C<sub>11</sub>H<sub>11</sub>NS<sub>8</sub>: C, 31.94; H, 2.68; N, 3.39. Found: C, 31.66; H, 2.05; N, 3.28.

**TTF 4e**

To a solution of **4a** (65 mg; 0.148 mmol) in 4 mL DMF under inert atmosphere was added dropwise a solution of caesium hydroxide (24.4 mg; 0.163 mmol) in 1 mL of degassed methanol. The mixture was stirred 30 min then a solution of cyanogen bromide (23 mg, 0.22 mmol) in 2 mL of degassed DMF was added. The mixture was stirred 1 hour and the reaction was quenched with 100 mL water, the organic phase was extracted with CH<sub>2</sub>Cl<sub>2</sub>, and dried over MgSO<sub>4</sub>. The solvent was evaporated *in vacuo* and the residue was purified by chromatography using CH<sub>2</sub>Cl<sub>2</sub> as eluent to afford **4e** as a red powder. Yield = 70% (*m* = 43 mg); Rf = 0.80 (SiO<sub>2</sub>, CH<sub>2</sub>Cl<sub>2</sub>); mp = 148 °C; <sup>1</sup>H NMR (300 MHz) δ 2.62 (s, 6H). <sup>13</sup>C NMR (75 MHz, CD<sub>2</sub>Cl<sub>2</sub>) δ (ppm) = 151.1 (C=C), 147.8 (C=N), 128.9 (C=C), 128.2 (C=C), 127.2 (C=C), 116.6 (CN), 110.8 (C=C), 106.9 (C=C), 19.3 (CH<sub>3</sub>), 19.2 (CH<sub>3</sub>). HRMS (ASAP) calcd for [C<sub>10</sub>H<sub>6</sub>N<sub>2</sub>S<sub>8</sub>]<sup>+</sup>: 409.82912. Found: 409.8091; anal. calcd for



C<sub>10</sub>H<sub>6</sub>N<sub>2</sub>S<sub>8</sub>: C, 29.25; H, 1.47; N, 6.82. Found: C, 29.73; H, 1.44; N, 6.32.

4 mL of dichloromethane was left at refluxed for 10 min. The solution was filtered and slow concentration of the solution afforded crystals of sufficient quality for X ray diffraction.

### Charge transfer salt

(4B)(TCNQF<sub>4</sub>). A mixture of 4B (10.16 mg, 0.028 mmol) and TCNQF<sub>4</sub> (7.66 mg, 0.028 mmol) in 15 mL of acetonitrile and 4 mL of dichloromethane was left at refluxed for 10 min. The solution was filtered and slow concentration of the solution afforded crystals of sufficient quality for X ray diffraction.

(4c)<sub>2</sub>(TCNQF<sub>4</sub>). A mixture of 4c (8.2 mg, 0.017 mmol) and TCNQF<sub>4</sub> (4.60 mg, 0.017 mmol) in 15 mL of acetonitrile and

### X-ray crystallographic analysis

Data were collected on a D8 VENTURE Bruker AXS diffractometer, equipped with a (CMOS) Photon 100 detector, for all the crystals except for 3d where data collection was performed on an APEXII Bruker-AXS diffractometer, using Mo K $\alpha$  radiation ( $\lambda = 0.71073 \text{ \AA}$ , multilayer monochromator). The structures were solved by dual-space algorithm using the SHELXT program,<sup>31</sup> and the refined with full-matrix least-

Table 5 Crystallographic data

Compound	2a	2e	2f	3d
CCDC	2245494	2245495	2245496	2245497
Formula	C <sub>7</sub> H <sub>4</sub> N <sub>2</sub> OS <sub>4</sub>	C <sub>5</sub> N <sub>2</sub> OS <sub>4</sub>	C <sub>5</sub> H <sub>3</sub> NOS <sub>4</sub>	C <sub>12</sub> H <sub>10</sub> N <sub>2</sub> S <sub>8</sub>
FW (g mol <sup>-1</sup> )	260.36	232.31	221.32	438.7
Crystal system	Triclinic	Monoclinic	Monoclinic	Monoclinic
Space group	P $\bar{1}$	C2/c	P2 <sub>1</sub> /c	P2 <sub>1</sub> /a
a (Å)	7.0683(15)	19.606(4)	9.1900(18)	14.4980(13)
b (Å)	8.6879(17)	3.8452(7)	10.0186(17)	7.5276(9)
c (Å)	9.462(2)	20.687(4)	8.6765(17)	16.6742(17)
$\alpha$	111.186(8)	90	90	90
$\beta$	108.771(8)	91.669(5)	98.049(7)	111.731(5)
$\gamma$	97.407(8)	90	90	90
V (Å <sup>3</sup> )	492.79(18)	1558.9(5)	791.0(3)	1690.4(3)
T (K)	150(2)	150(2)	150(2)	296(2)
Z	2	8	4	4
D <sub>calc</sub> (g cm <sup>-3</sup> )	1.755	1.98	1.859	1.724
$\mu$ (mm <sup>-1</sup> )	0.926	1.158	1.132	1.05
Total refls.	5511	5045	1775	14 546
Abs. Corr.	Multi-scan	Multi-scan	Multi-scan	Multi-scan
Uniq. refls. ( $R_{int}$ )	2195(0.0356)	1709(0.0567)	1775	3876(0.0406)
Unique refls. ( $I > 2\sigma(I)$ )	2084	1399	1607	2851
$R_1, wR_2$	0.0274, 0.0766	0.0571, 0.1197	0.0385, 0.0981	0.0374, 0.0894
$R_1, wR_2$ (all data)	0.0287, 0.0787	0.0738, 0.1257	0.0455, 0.1036	0.060, 0.1013
GoF	1.029	1.09	1.167	1.049

Compound	4a	4b	4e	(4b)(TCNQF <sub>4</sub> )	(4c) <sub>2</sub> (TCNQF <sub>4</sub> )
CCDC	2245498	2245499	2245500	2245501	2245502
Formula	C <sub>12</sub> H <sub>10</sub> N <sub>2</sub> S <sub>8</sub>	C <sub>9</sub> H <sub>7</sub> NS <sub>7</sub>	C <sub>10</sub> H <sub>6</sub> N <sub>2</sub> S <sub>8</sub>	C <sub>21</sub> H <sub>7</sub> F <sub>4</sub> N <sub>5</sub> S <sub>7</sub>	C <sub>30</sub> H <sub>12</sub> F <sub>4</sub> I <sub>2</sub> N <sub>6</sub> S <sub>14</sub>
FW (g mol <sup>-1</sup> )	438.70	353.58	410.65	629.74	1235.10
Crystal system	Triclinic	Triclinic	Triclinic	Triclinic	Triclinic
Space group	P $\bar{1}$	P $\bar{1}$	P $\bar{1}$	P $\bar{1}$	P $\bar{1}$
a (Å)	6.0133(3)	7.906(2)	7.4506(12)	7.1063(15)	7.2339(10)
b (Å)	10.3719(7)	8.704(3)	8.1175(12)	12.405(3)	10.7451(15)
c (Å)	14.1989(9)	11.633(3)	13.345(2)	13.462(4)	13.7344(19)
$\alpha$	84.691(2)	100.130(10)	73.335(5)	100.797(12)	77.886(5)
$\beta$	79.633(2)	101.742(10)	87.672(6)	91.933(13)	87.003(5)
$\gamma$	85.606(2)	113.220(10)	81.049(6)	92.390(9)	72.421(5)
V (Å <sup>3</sup> )	865.76(9)	690.4(3)	763.8(2)	1163.7(6)	995.0(2)
T (K)	296(2)	296(2)	150(2)	150(2)	150(2)
Z	2	2	2	2	1
D <sub>calc</sub> (g cm <sup>-3</sup> )	1.683	1.701	1.786	1.797	2.061
$\mu$ (mm <sup>-1</sup> )	1.026	1.116	1.156	0.735	2.370
Total refls.	17 937	14 575	21 489	24 703	20 058
Abs. Corr.	Multi-scan	Multi-scan	Multi-scan	Multi-scan	Multi-scan
Uniq. refls. ( $R_{int}$ )	3918(0.0269)	3075(0.0303)	3500(0.0316)	5303(0.0589)	4514(0.0450)
Unique refls. ( $I > 2\sigma(I)$ )	3494	2738	3295	4361	3913
$R_1, wR_2$	0.0306, 0.0807	0.0274, 0.0687	0.0274, 0.0785	0.0436, 0.0899	0.0382, 0.0895
$R_1, wR_2$ (all data)	0.0349, 0.0839	0.0319, 0.0727	0.0291, 0.0806	0.0589, 0.0964	0.0469, 0.0940
GoF	1.062	1.042	1.039	1.009	1.081





square methods based on  $F^2$  (SHELXL).<sup>32</sup> All non-hydrogen atoms were refined with anisotropic atomic displacement parameters. H atoms were finally included in their calculated positions. Crystallographic data on X-ray data collection and structure refinements are given in Table 5. CCDC 2245494–2245502 contain the supplementary crystallographic data for this paper.

### Theoretical modeling

Electrostatic Surface Potential calculations were carried out on the optimized geometry of the molecules (with density functional theory using the Gaussian 09 Revision D.01 software, the B3LYP functional and the 6-31+G\*\* basis set for all atoms and the LANLdp basis set for iodine). GaussView 5.0.9 was used to generate the figures.

### Conflicts of interest

There are no conflicts to declare.

### Acknowledgements

This work was financially supported by Université de Rennes 1 & through a PhD grant (to H. H.). This work was granted access to the HPC resources of CEA-TGCC under the allocation 2023 – AD010814136 awarded by GENCI.

### References

- (a) J. Ferraris, D. O. Cowan, V. T. Walatka and J. H. Perlstein, *J. Am. Chem. Soc.*, 1973, **95**, 948–949; (b) L. B. Coleman, M. J. Cohen, D. J. Sandman, F. G. Yamagishi, A. F. Garito and A. J. Heeger, *Solid State Commun.*, 1973, **12**, 1125–1132.
- P. Batail, Special issue on Molecular Conductors, *Chem. Rev.*, 2004, **104**, 4887–5781.
- N. Martín and J.-L. Segura, *Angew. Chem., Int. Ed.*, 2001, **40**, 1372–1409.
- D. Canevet, M. Sallé, G. Zhang, D. Zhang and D. Zhu, *Chem. Commun.*, 2009, 2245–2269.
- M. B. Nielsen, C. Lomholt and J. Becher, *Chem. Soc. Rev.*, 2000, **29**, 153–164.
- H.-Y. Wang, L. Cui, J.-Z. Xie, C.-F. Leong, D. M. D'Alessandro and J.-L. Zuo, *Coord. Chem. Rev.*, 2017, **345**, 342–361.
- H. Jiang, P. Hu, J. Ye, K. K. Zhang, Y. Long, W. Hu and C. Kloc, *J. Mater. Chem. C*, 2018, **6**, 1884–1902.
- E. Arunan, G. R. Desiraju, R. A. Klein, J. Sadlej, S. Scheiner, I. Alkorta, D. C. Clary, R. H. Crabtree, J. J. Dannenberg, P. Hobza, H. G. Kjaergaard, A. C. Legon, B. Mennucci and D. J. Nesbitt, *Pure Appl. Chem.*, 2011, **83**, 1637–1641.
- M. R. Bryce, *J. Mater. Chem.*, 1995, **5**, 1481–1496.
- T. Isono, H. Kamo, A. Ueda, K. Takahashi, A. Nakao, R. Kumai, H. Nakao, K. Kobayashi, Y. Murakami and H. Mori, *Nat. Commun.*, 2013, **4**, 1344–1349.
- (a) G. Cavallo, P. Metrangolo, R. Milani, T. Pilati, A. Priimagi, G. Resnati and G. Terraneo, *Chem. Rev.*, 2016, **116**, 2478–2601; (b) L. C. Gilday, S. W. Robinson, T. A. Barendt, M. J. Langton, B. R. Mullaney and P. D. Beer, *Chem. Rev.*, 2015, **115**, 7118–7195.
- (a) M. Fourmigué and P. Batail, *Chem. Rev.*, 2004, **11**, 5379–5418; (b) O. Jeannin, E. Canadell, P. Auban-Senzier and M. Fourmigué, *Chem. Commun.*, 2016, **52**, 308–311; (c) A. Frąckowiak, R. Świetlik, L. Maulana, D. Liu, M. Dressel, O. Jeannin and M. Fourmigué, *J. Phys. Chem. C*, 2020, **124**, 5552–5558.
- (a) R. Oliveira, S. Groni, C. Fave, M. Branca, F. Mavre, D. Lorcy, M. Fourmigué and B. Schöllhorn, *Phys. Chem. Chem. Phys.*, 2016, **18**, 15867–15873; (b) R. Oliveira, S. Groni, A. Vacher, F. Barrière, D. Lorcy, M. Fourmigué, E. Maisonhaute, B. Schöllhorn and C. Fave, *ChemistrySelect*, 2018, **3**, 8874–8880; (c) H. Hijazi, A. Vacher, S. Groni, D. Lorcy, E. Levillain, C. Fave and B. Schöllhorn, *Chem. Commun.*, 2019, **55**, 1983–1986.
- R. Gleiter, G. Haberhauer, D. B. Werz, F. Rominger and C. Bleiholder, *Chem. Rev.*, 2018, **118**, 2010–2041.
- (a) O. Jeannin, E. W. Reinheimer, P. Foury-Leylekian, J. P. Pouget, P. Auban-Senzier, E. Trzop, E. Collet and M. Fourmigué, *IUCrJ*, 2018, **5**, 361–372; (b) M. Beau, O. Jeannin, M. Fourmigué, P. Auban-Senzier, F. Barrière and I.-R. Jeon, *CrystEngComm*, 2022, **24**, 7535–7539.
- P. Politzer and S. J. Murray, *Crystals*, 2017, **7**, 212–226.
- (a) A. Filatre-Furcate, P. Auban-Senzier, M. Fourmigué, T. Roisnel, V. Dorcet and D. Lorcy, *Dalton Trans.*, 2015, **44**, 15683–15689; (b) A. Filatre-Furcate, T. Roisnel and D. Lorcy, *J. Organomet. Chem.*, 2016, **819**, 182–188.
- (a) H. Hachem, Z. Xu, N. Bellec, O. Jeannin, P. Auban-Senzier, T. Guizouarn, M. Fourmigué and D. Lorcy, *Dalton Trans.*, 2018, **47**, 6580–6589; (b) H. Hachem, N. Bellec, M. Fourmigué and D. Lorcy, *Dalton Trans.*, 2020, **49**, 6056–6064.
- H. Hachem, O. Jeannin, M. Fourmigué, F. Barrière and D. Lorcy, *CrystEngComm*, 2020, **22**, 3579–3587.
- N. Svenstrup, K. M. Rasmussen, T. K. Hansen and J. Becher, *Synthesis*, 1994, 809–912.
- (a) M. Narita and C. U. Jr Pittman, *Synthesis*, 1976, 489–514; (b) A. Krief, *Tetrahedron*, 1986, **42**, 1209–1252; (c) G. Schukat, A. M. Richter and E. Fanghänel, *Sulfur Rep.*, 1987, **7**, 155–231.
- T. Konoike, K. Namba, T. Shinida, K. Sakaguchi, G. C. Papavassiliou, K. Murata and Y. Ohfuné, *Synlett*, 2001, **9**, 1476–1478.
- Y. Le Gal, A. Colas, F. Barrière, V. Dorcet, T. Roisnel and D. Lorcy, *CrystEngComm*, 2019, **21**, 1934–1939.
- R. P. Shibaeva and E. B. Yagubskii, *Chem. Rev.*, 2004, **104**, 5347–5378.
- J. Liefbrig, O. Jeannin, A. Frąckowiak, I. Oleniczak, R. Świetlik, S. Dahaoui, E. Aubert, E. Espinosa, P. Auban-Senzier and M. Fourmigué, *Chem. – Eur. J.*, 2013, **19**, 14804–14813.
- T. J. Kistenmacher, T. J. Emge, A. N. Bloch and D. O. Cowan, *Acta Crystallogr., Sect. B: Struct. Crystallogr. Cryst. Chem.*, 1982, **38**, 1193–1199.
- H. Miyasaka, N. Motokawa, S. Matsunaga, M. Yamashita, K. Sugimoto, T. Mori, N. Toyota and K. R. Dunbar, *J. Am. Chem. Soc.*, 2010, **132**, 1532–1544.





- 28 S. A. O'Kane, R. Clérac, H. Zhao, X. Ouyang, J. R. Galan-Mascaros, R. Heintz and K. R. Dunbar, *J. Solid State Chem.*, 2000, **152**, 159–173.
- 29 P. Hu, H. Li, Y. Li, H. Jiang and C. Kloc, *CrystEngComm*, 2017, **19**, 618–624.
- 30 R. F. W. Bader, *Chem. Rev.*, 1991, **91**, 893–928.
- 31 G. M. Sheldrick, *Acta Crystallogr., Sect. A: Found. Adv.*, 2015, **71**, 3–5.
- 32 G. M. Sheldrick, *Acta Crystallogr., Sect. C: Struct. Chem.*, 2015, **71**, 3–5.

